Available online at www.sciencedirect.com
ScienceDirect
International Journal of Heat and Mass Transfer 51 (2008) 434–444
International Journal of HEAT and MASS TRANSFER
www.elsevier.com/locate/ijhmt

Entrance heat transfer in rectangular ducts with constant axial energy input

A. Haji-Sheikh [a,*], J.V. Beck [b]

[a] Department of Mechanical and Aerospace Engineering, The University of Texas at Arlington, Arlington, TX 76019-0023, United States
[b] Department of Mechanical Engineering, Michigan State University, East Lansing, MI 48824-1226, United States

Received 8 September 2006; received in revised form 21 May 2007
Available online 31 July 2007

Abstract

The study of heat transfer in the entrance region of ducts with different cross-sections is important in engineering practice. This paper considers laminar, hydrodynamically fully developed flow in the thermal entrance regions of rectangular passages, emphasizing heat transfer aspects. By having a prescribed heating or cooling rate and considering the wall temperature to depend on the axial coordinate alone, the temperature solution leads to an integral equation. Solution of this equation is found using an inverse technique to determine the temperature at the walls. For verification purposes, an asymptotic solution is developed which produces results that agree very well with those from the inverse analysis. The results include a correlation and computed values of the Nusselt number at entrance locations, for rectangular ducts with different aspect ratios.

Keywords: Convection; Heat transfer; Thermal entrance; Rectangular ducts; Inverse analysis

1. Introduction

Studies of heat transfer to flow in ducts with different cross-section profiles are reported in the past and they are currently available in the literature. A survey of earlier work describing heat transfer in various-shaped ducts is in Shah and London [1] and Kays and Perkin [2]. Summarized information on the heat transfer within these passages, available in [3–5], is an indicative of their practical values. In particular, the heat transfer to flow through rectangular passages is of interest in heat exchanger applications, electronic cooling, and others.

The method of determination of temperature field in rectangular channels, with classical boundary conditions, is well documented in the literature. Three types of boundary conditions are classified [1]. The locally constant wall temperature case, known as the T boundary condition, has direct solutions. The locally constant wall heat flux at the boundaries, classified as H2 boundary condition, also has direct solutions for different rectangular ducts. Another model, called H1 boundary condition [1], has the heat flux per unit length being uniform while the wall temperature remains a function of the axial coordinate, uniform along the perimeter of the ducts [2,3]. This latter case does not have a direct solution in the thermally developing region; therefore, the inverse methodology becomes a useful tool to study the heat transfer phenomena in ducts with various cross-section profiles.

The objective of this study is the determination of the wall temperature of a duct when there is a uniform energy input in the axial direction. Although rectangular ducts are selected to illustrate the temperature solution methodology, similar analyses apply to other passages. When the wall temperature depends on the axial coordinate alone, it needs to be estimated numerically using an inverse methodology. A solution begins by finding the velocity field from the solution of the momentum equation. Next, the energy equation should be utilized in order to find the temperature distribution. During these formulations, the flow is considered to be

* Corresponding author. Tel.: +1 817 272 2010; fax: +1 817 272 2952.
E-mail address: haji@uta.edu (A. Haji-Sheikh).

0017-9310/$ - see front matter © 2007 Elsevier Ltd. All rights reserved.
doi:10.1016/j.ijheatmasstransfer.2007.05.012

Nomenclature

a, b	dimensions of rectangle, see Fig. 1
a_{ij}	elements of matrix **A**
A	cross-section area, $a \times b$
A_s	surface area
A	matrix of coefficients
$\bar{b}$	b/a
c_p	specific heat, J/kg K
c_j	constants, members of **C**
C	dimensionless velocity coefficient
C	vector of coefficients c_j
d_{mj}	coefficient in matrix **D**
D_h	hydraulic diameter, $4ab/(a+b)$, m
D	matrix with coefficients d_{mj}
e	coefficient, Eq. (37b)
h	heat transfer coefficient, W/m^2 K
j	index
f_j	basis functions in weighted residual method
k	thermal conductivity, W/m K
m, n	indices
Nu_D	hD_h/k
p	pressure, Pa
Pe	Peclet number, Ua/α
Pr	Prandtl number, $\mu c_p/k$
q_w	wall heat flux, W/m^2
Q_w	total heat flux, W
T_i	initial temperature, K
T_m	mean or bulk temperature, K
T_w	wall temperature, K
u	velocity, m/s
U	average velocity, m/s
$\bar{u}$, $\overline{U}$	dimensionless velocities, see Eqs. (2) and (7)
V	volume, m^3
$\hat{x}$	axial coordinate, m
x^+	$2(\hat{x}/D_h)/(PrRe_D)$
x	$(\hat{x}/a)/Pe$
y, z	$\hat{y}/a$ and $\hat{z}/a$
$\hat{y}, \hat{z}$	coordinates, m

Greek symbols

α	thermal diffusivity, m^2/s
β_n	eigenvalues
γ_m	eigenvalue
δ	a constant
Γ	a product of two function, Eq. (25)
θ	temperature function, see Eq. (12)
θ^*	temperature function $\theta - \theta_w$
μ	viscosity coefficient, N s/m^2
ϕ_j	basis functions for θ_w
Φ_m	special function, see Eq. (27c)
Ψ_m	special function, see Eq. (27c)
ω_i	elements of vector Ω
$\boldsymbol{\Omega}$	vector of known values ω_i

Subscripts

Calc	calculated value
FD	fully developed condition
m	average value or index
w	wall condition

unidirectional and hydrodynamically fully developed. Under these conditions, the velocity field in rectangular ducts has an exact series solution; two different solutions are presented in Section 2. Also, Section 3.1 describes an exact series solution for the fully developed temperature field in these passages when the wall temperature and the mean (or bulk) temperature change linearly with the axial coordinate $\hat{x}$. However, the computation of temperature in the thermally developing region requires a numerical procedure. This numerical study of the temperature field includes two different methods of analyses. The first one in Section 3.2 considers temperature penetration away from the wall to be small and this leads to an asymptotic analytical solution. The second solution requires a numerical inverse procedure for the estimation of the unknown wall temperature; details are in Section 3.3. The numerical results from this study are included in Section 4.

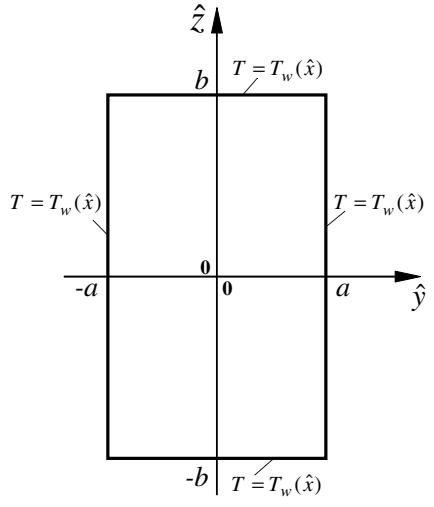

Fig. 1. Schematic of rectangular cross-section with imposed boundary conditions.

2. Velocity field in a rectangular duct

For hydrodynamically fully developed laminar flow passing through a rectangular duct, depicted in Fig. 1, the momentum equation in its reduced form is

$$\mu\left(\frac{\partial^2 u}{\partial \hat{y}^2}+\frac{\partial^2 u}{\partial \hat{z}^2}\right)-\frac{\partial p}{\partial \hat{x}}=0 \tag{1}$$

where μ is the fluid viscosity. If the flow is hydrodynamically fully developed, the pressure gradient $\partial p/\partial \hat{x}$ is a constant. Using the duct dimension a, in Fig. 1, as the characteristic length, the following dimensionless quantities are selected: $y = \hat{y}/a$, $z = \hat{z}/a$, and $\bar{u} = \mu u/(-a^2 \partial p/\partial \hat{x})$. Then, Eq. (1) becomes

$$\left(\frac{\partial^2 \bar{u}}{\partial y^2} + \frac{\partial^2 \bar{u}}{\partial z^2}\right) + 1 = 0 \tag{2}$$

subject to the condition of $\bar{u} = 0$ at the wall. The solution for Eq. (2) has two different forms and both are used in the following formulations.

A rapidly converging series solution of Eq. (2) with a single summation is obtainable by a well-known eigenfunction expansion approach [6]

$$\bar{u} = \sum_{n=1}^{\infty} F_n(z)\cos(\beta_n y) \tag{3}$$

with $\beta_n = (n - 1/2)\pi$, and

$$F_n(z) = \frac{2(-1)^{n-1}}{\beta_n^3}\left[1 - \frac{\cosh \beta_n z}{\cosh \beta_n \bar{b}}\right] \tag{4}$$

After substitution of $F_n(z)$ in Eq. (3) and using a known identity, it can be written as

$$\bar{u} = \frac{1}{2}(1 - y^2) - 2\sum_{n=1}^{\infty} \frac{(-1)^{n-1}\cos(\beta_n y)}{\beta_n^3} \frac{e^{-\beta_n(\bar{b}-z)} + e^{-\beta_n(\bar{b}+z)}}{1 + e^{-2\beta_n \bar{b}}} \tag{5}$$

Next, it is common to determine the mean velocity

$$U = \frac{1}{A}\int_A u \, dA \tag{6}$$

and obtain the value of $\overline{U} = \mu U/(-a^2 \partial p/\partial \hat{x})$; that is

$$\overline{U} = \frac{2}{\bar{b}}\sum_{n=1}^{\infty} \frac{\beta_n \bar{b} - \tanh(\beta_n \bar{b})}{\beta_n^5} = \frac{1}{3} - \frac{2}{\bar{b}}\sum_{n=1}^{\infty} \frac{\tanh(\beta_n \bar{b})}{\beta_n^5} \tag{7}$$

Then, the final form of the normalized velocity is

$$\frac{u}{U} = \frac{\bar{u}}{\overline{U}} = \frac{\sum_{n=1}^{\infty} F_n(z)\cos(\beta_n y)}{\frac{1}{3} - \frac{2}{\bar{b}}\sum_{n=1}^{\infty} \frac{\tanh(\beta_n \bar{b})}{\beta_n^5}} \tag{8}$$

where $\bar{b} = b/a$. This rapidly converging solution is useful when computing the velocity gradient at the walls and it is used for finding the temperature solution at very small x values.

Alternatively, one can obtain a direct solution of the classical Poisson equation, Eq. (2), by considering the velocity field to be

$$\bar{u} = \sum_{n=1}^{\infty}\sum_{m=1}^{\infty} a_{mn}\cos(\beta_n y)\cos(\gamma_m z) \tag{9}$$

where $\beta_n = (n - 1/2)\pi$, $\gamma_m = (m - 1/2)\pi/\bar{b}$ and a_{mn} is the unknown Fourier coefficient. The substitution of $\bar{u}$ in Eq. (2) and after the application of the orthogonality condition a_{mn} becomes

$$a_{mn} = \frac{4(-1)^{m+n}}{\bar{b}\beta_n \gamma_m(\beta_n^2 + \gamma_m^2)} \tag{10}$$

with the average velocity as given by Eq. (7). This form of the velocity field becomes useful when computing the heat transfer coefficient in the thermally fully developed region.

3. Energy equation and temperature solution

The following formulations are for laminar flow with fully developed velocity field passing through a rectangular duct heated at a constant rate in the axial direction. For H1 boundary condition, the wall temperature $T_w(\hat{x})$ remains a function of the axial coordinate $\hat{x}$, independent of $\hat{y}$ and $\hat{z}$. For the determination of temperature, axial heat conduction is neglected. Therefore, the energy equation for a sufficiently large Peclet number is

$$\frac{\partial^2 T}{\partial \hat{y}^2} + \frac{\partial^2 T}{\partial \hat{z}^2} = \frac{1}{\alpha}u(\hat{y},\hat{z})\frac{\partial T}{\partial \hat{x}} \tag{11}$$

subject to the specified set of boundary conditions. At the thermal entrance region, the inlet temperature is T_i = constant. When $\hat{x} \geqslant 0$, the average wall heat flux is $q_w = dQ_w/dA_s$ where $dA_s = 4(a + b)d\hat{x}$ is the surface area element. In the subsequent formulations, two different dimensionless temperatures are used; the first one is

$$\theta = \frac{T(\hat{y},\hat{z};\hat{x}) - T_i}{(q_w a/k)} \tag{12}$$

where a is the characteristic length, as shown is Fig. 1, and k is the fluid thermal conductivity. When θ is defined by Eq. (12) but with dimensionless coordinates $x = \alpha\hat{x}/(Ua^2)$, $y = \hat{y}/a$ and $z = \hat{z}/a$, Eq. (11) would take the following form:

$$\frac{\partial^2 \theta}{\partial y^2} + \frac{\partial^2 \theta}{\partial z^2} = \left(\frac{u}{U}\right)\frac{\partial \theta}{\partial x} \tag{13}$$

Accordingly, the entrance condition becomes $\theta(y,z,0) = 0$ while the wall condition is $\theta = \theta_w(x)$. For the case of prescribed heat flux, the mean or bulk temperature is known a priori by applying energy balance to a material element; that is $\rho U a b c_p dT_m = q_w(a + b)d\hat{x}$. Also, by definition, the mean or bulk temperature in the dimensionless space $\theta_m(x)$ is

$$\theta_m(x) = \frac{1}{1 \times \bar{b}}\int_0^1\int_0^{\bar{b}} \left(\frac{u}{U}\right)\theta(y,z;x)\,dz\,dy \tag{14}$$

Accordingly when q_w = constant, the left side of this equation varies linearly with x. Since $\theta(y,z;x)$ within the integral is the unknown, an inverse methodology is a suitable scheme for its determination. However, prior to determination temperature within the thermal entrance region, it is appropriate to obtain the temperature solution, $\theta(y,z;\infty)$, under fully developed thermal condition.

3.1. Fully developed thermal solution

This special solution considers uniform energy input per unit length of a passage while maintaining a wall temperature $T_w(\hat{x})$ that depends only on the axial coordinate $\hat{x}$. This case is expected when the walls of a passage are orthotropic with a relatively high thermal conductivity in the directions perpendicular to x-axis. Under fully developed thermal condition, the temperature profiles become similar. Furthermore, with the average wall heat flux designated as q_w, the aforementioned conditions require that $\partial T/\partial\hat{x} = \partial T_b/\partial\hat{x} = q_w(a+b)/(abc_p\rho U)$. After inserting this value of $\partial T/\partial\hat{x}$ in Eq. (11) and then replacing T using the relation $T = T_w + \theta^*(q_w a/k)$, in dimensionless space, it becomes

$$\left(\frac{\partial^2\theta^*}{\partial y^2}+\frac{\partial^2\theta^*}{\partial z^2}\right)=\left(\frac{4a}{D_h}\frac{u}{U}\right)=\left(\frac{4a}{D_h}\frac{\bar{u}}{\overline{U}}\right) \tag{15}$$

where $D_h = 4A/C = 4ab/(a+b)$ is the hydraulic diameter and θ^* is the second dimensionless temperature. The solution of Eq. (15) is obtainable from the relation

$$\theta^*(y,z)=\frac{1}{\overline{U}}\sum_{n=1}^{\infty}\sum_{m=1}^{\infty}c_{mn}\cos(\beta_n y)\cos(\gamma_m z) \tag{16}$$

where $\overline{U}$ is defined in Eq. (7). Next, the function θ^* from Eq. (16) and the dimensionless velocity $\bar{u}$, from Eqs. (9) and (10), should be substituted in Eq. (15). Then, the application of orthogonality condition yields

$$c_{mn}=-\left(\frac{4a}{D_h}\right)\frac{a_{mn}}{(\beta_n^2+\gamma_m^2)} \tag{17}$$

Based on the definition of heat transfer coefficient $h = q_w/(T_w - T_m)$ and using the definition, $\theta_m^* = (T_m - T_w)/(q_w a/k)$, one gets $Nu_a = ha/k = -1/\theta_m^*$. Then, the substitution of θ^* from Eq. (16) in the modified form of Eq. (14) leads to a rapidly converging series solution

$$\theta_m^*=\sum_{n=1}^{\infty}\sum_{m=1}^{\infty}\frac{a_{mn}c_{mn}}{4\overline{U}^2}=\frac{-a}{D_h(\overline{U}\bar{b})^2}\sum_{n=1}^{\infty}\sum_{m=1}^{\infty}\frac{16}{\beta_n^2\gamma_m^2(\beta_n^2+\gamma_m^2)^3} \tag{18}$$

for the bulk temperature. Therefore, the Nusselt number is

$$\frac{ha}{k}=-\frac{1}{\theta_m^*}\quad\text{and}\quad Nu_D=-\left(\frac{D_h}{a}\right)\frac{1}{\theta_m^*} \tag{19}$$

3.2. Asymptotic temperature solution at very small x

At an extremely small distance from the location where heating begin, it is possible to simplify the energy equation to assume the following reduced forms:

$$\frac{\partial^2 T}{\partial\hat{y}^2}=\frac{1}{\alpha}u(\hat{y},\hat{z})\frac{\partial T}{\partial\hat{x}} \tag{20a}$$

near $\hat{y} = -a$ wall and

$$\frac{\partial^2 T}{\partial\hat{z}^2}=\frac{1}{\alpha}u(\hat{y},\hat{z})\frac{\partial T}{\partial\hat{x}} \tag{20b}$$

near $\hat{z} = -b$ wall. Therefore, $\hat{z}$ serves as a parameter when solving Eq. (20a) and $\hat{y}$ serve as a parameter in Eq. (20b). Since the solution for these two equations is similar, the following solution steps are for Eq. (20a).

When the temperature penetration is in the vicinity of the wall, the velocity is nearly a linear function of the distance from the wall, $\hat{y}$. Then, the velocity near the wall can be approximated as

$$u\cong C_y(\hat{z})(\hat{y}+a),\quad\text{and}\quad C_y(\hat{z})=\left.\frac{\partial u(\hat{y},\hat{z};\hat{x})}{\partial\hat{y}}\right|_{\hat{y}=-a} \tag{21}$$

For this velocity, Eq. (20a) takes the form

$$\alpha\frac{\partial^2 T}{\partial\hat{y}^2}=C_y(\hat{z})(\hat{y}+a)\frac{\partial T}{\partial\hat{x}} \tag{22}$$

with the inlet conditions $T(\hat{y},\hat{z};0) = T_i$ and the boundary condition

$$-k\left.\frac{\partial T}{\partial\hat{y}}\right|_{\hat{y}=-a}=q_w \tag{23}$$

at the walls.

Using the definition for dimensionless temperature, as given by Eq. (12), makes Eq. (22) to become

$$\alpha\frac{\partial^2\theta}{\partial\hat{y}^2}=C_y(\hat{z})(\hat{y}+a)\frac{\partial\theta}{\partial\hat{x}} \tag{24}$$

The solution of Eq. (24) is obtainable by utilization of the Laplace transform technique and accordingly

$$\alpha\frac{\partial^2\bar{\theta}}{\partial\hat{y}^2}=C_y(\hat{z})(\hat{y}+a)s\bar{\theta} \tag{25}$$

where $\bar{\theta}$ is the Laplace transform θ with respect to $\hat{x}$. Now, to change the other variable, let

$$\eta=(\hat{y}+a)\left(\frac{C_y(\hat{z})s}{\alpha}\right)^{1/3}\quad\text{or}\quad\hat{y}+a=\eta\left(\frac{\alpha}{C_y(\hat{z})s}\right)^{1/3} \tag{26}$$

and this makes

$$\frac{\partial^2\bar{\theta}}{\partial\eta^2}=\eta\bar{\theta} \tag{27}$$

with the boundary conditions being the Laplace transform of Eq. (23)

$$\left.\frac{d\bar{\theta}}{d\eta}\right|_{\eta=0}=-\frac{1}{s^{4/3}}\left(\frac{\alpha}{C_y(\hat{z})a^3}\right)^{1/3} \tag{28}$$

and the condition at infinity of $\bar{\theta}$ being finite.

Eq. (27) is called the Airy ordinary differential equation [7, p. 446] and its solutions $Ai(\eta]$ and $Bi(\eta]$ are available in symbolic computer packages; e.g., in Mathematica [8], they are designated as Airy$Ai[\eta]$ and Airy$Bi[\eta]$. The general solution of Eq. (27) is

$$\bar{\theta}(\eta)=C_1 Ai(\eta)+C_2 Bi(\eta) \tag{29}$$

Since Bi goes to infinity as η goes to infinity, C_2 must be zero. The boundary condition given by Eq. (28) yields the value of C_1; then

$$\bar{\theta}(\eta) = -\frac{1}{s^{4/3}}\left(\frac{\alpha}{C_y(\hat{z})a^3}\right)^{1/3}\frac{Ai(\eta)}{Ai'(0)} \tag{30}$$

The inverse Laplace transform of Eq. (30), when $\eta = 0$, yields the wall temperature

$$\theta(-a,\hat{z};\hat{x}) = -\frac{1}{\Gamma(4/3]}\left(\frac{\alpha\hat{x}}{C_y(\hat{z})a^3}\right)^{1/3}\frac{Ai(0)}{Ai'(0)} = 1.5361\left(\frac{\alpha\hat{x}}{C_y(\hat{z})a^3}\right)^{1/3} \tag{31a}$$

Similarly, using the same algebraic steps, the wall temperature along $\hat{z} = -b$ surface is

$$\theta(\hat{y},-b;\hat{x}) = -\frac{1}{\Gamma(4/3]}\left(\frac{\alpha\hat{x}}{C_z(\hat{y})a^3}\right)^{1/3}\frac{Ai(0)}{Ai'(0)} = 1.5361\left(\frac{\alpha\hat{x}}{C_z(\hat{y})a^3}\right)^{1/3} \tag{31b}$$

In the determination of Eq. (31a), it is assumed that temperature penetration from the wall in the adjacent fluid, at any $\hat{x}$ location, is a function $\hat{y}$ alone. This condition is similar to that when applying this procedure to parallel plate channels where the wall temperature and wall heat flux depend on $\hat{x}$ alone. However, the rectangular ducts with constant axial energy input may have the wall temperature and wall heat flux varying along the perimeter at any given $\hat{x}$ location. Two limiting conditions are defined in [1] to address this situation: The H1 case assumes T_w to depend on $\hat{x}$ alone while circumferentially average heat flux at this $\hat{x}$ location is q_w. The H2 case assumes q_w to be locally constant while the circumferentially average temperature at any $\hat{x}$ location is $T_w(\hat{x})$. Accordingly, these two limiting cases would modify the working relations for each of these two cases. For the H1 case, having a constant $T_w = T_w(\hat{x})$, the average heat flux is

$$q_w(\hat{x}) = \frac{1}{2a+2b}\left[\int_{-b}^{b} q_{w,y}(\hat{z};\hat{x})\mathrm{d}\hat{z} + \int_{-a}^{a} q_{w,z}(\hat{y};\hat{x})\mathrm{d}\hat{y}\right] \tag{32a}$$

Then, the wall heat flux values within these integrals are obtainable, using Eqs. (31a,b), as

$$q_{w,y}(\hat{z})a/k = (T_w - T_i)[C_y(\hat{z})a^3/(\alpha\hat{x})]^{1/3}/1.5361,$$
$$q_{w,z}(\hat{y})a/k = (T_w - T_i)[C_z(\hat{y})a^3/(\alpha\hat{x})]^{1/3}/1.5361,$$

to be inserted into Eq. (32a) for the H1 case

$$\frac{q_w a}{k} = \frac{T_w - T_i}{2a+2b}\frac{1}{1.5361}\left\{\int_{-b}^{b}\left(\frac{C_y(\hat{z})a^3}{\alpha\hat{x}}\right)^{1/3}\mathrm{d}\hat{z} + \int_{-a}^{a}\left(\frac{C_z(\hat{y})a^3}{\alpha\hat{x}}\right)^{1/3}\mathrm{d}\hat{y}\right\} \tag{32b}$$

Furthermore, Eq. (32b) can be rewritten as

$$\frac{q_w a}{k} = \frac{T_w - T_i}{2a+2b}\frac{1}{1.5361}\left(\frac{a^3}{\alpha\hat{x}}\right)^{1/3} \times\left\{\int_{-b}^{b}[C_y(\hat{z})]^{1/3}\mathrm{d}\hat{z} + \int_{-a}^{a}[C_z(\hat{y})]^{1/3}\mathrm{d}\hat{y}\right\} \tag{32c}$$

The term within the braces has a constant value for a given aspect ratio b/a. For convenience of formulations, let

$$C^{1/3} = \frac{1}{a+b}\left\{\int_0^b [aC_y(\hat{z})/U]^{1/3}\mathrm{d}\hat{z} + \int_0^a [aC_z(\hat{y})/U]^{1/3}\mathrm{d}\hat{y}\right\} \tag{33}$$

and this simplifies the computation of wall temperature for the H1 case.

Alternatively, for the H2 case, $q_w = q_w(\hat{x})$ is independent of $\hat{y}$ and $\hat{z}$ while the average wall temperature is

$$T_w(\hat{x}) = \frac{1}{2a+2b}\left[\int_{-b}^{b} T_{w,y}(\hat{z};\hat{x})\mathrm{d}z + \int_{-a}^{a} T_{w,z}(\hat{y};\hat{x})\mathrm{d}\hat{y}\right] \tag{34}$$

Then, a similar procedure would provide the following effective C coefficient by directly averaging Eqs. (31a,b); that is, for the H2 case the expression is

$$C^{-1/3} = \frac{1}{a+b}\left\{\int_0^b [aC_y(\hat{z})/U]^{-1/3}\mathrm{d}\hat{z} + \int_0^a [aC_z(\hat{y})/U]^{-1/3}\mathrm{d}\hat{y}\right\} \tag{35}$$

For either H1 or H2 case, at very small values of x, the working relation is

$$\frac{T_w - T_i}{q_w a/k} = 1.5361\left(\frac{x}{C}\right)^{1/3} \tag{36a}$$

where $x = (\hat{x}/a)/Pe$ and $Pe = aU/\alpha$. Since at very small x values, $T_m \cong T_i$, then using the definition of $h = q_w/(T_w - T_m)$, Eq. (36a) yields the dimensionless heat transfer coefficient

$$\frac{ha}{k} = \left[1.5361\left(\frac{x}{C}\right)^{1/3}\right]^{-1} \tag{36b}$$

For convenience, in subsequent numerical simulation, the parameter C is computed for both H1 and H2 cases at different b/a values and the results are in Table 1. They show that both C values are relatively large when $b/a = 1$, they reduce monotonically, pass through minimums, and then they asymptotically approach 3 for parallel plate channels. This can also be demonstrated by examining the plotted values in Fig. 2. It is interesting to note that $h(2a)/k$, for the H1 case under the fully developed thermal condition, Eq. (19), has a similar behavior as can be seen from data appearing in Table 1 and plotted in Fig. 2. The quantity $h(2a)/k$ has a minimum of 3.0923 when $b/a = 1.97$ while the minimum of C (for H1) is located near $b/a = 3$ and the minimum of C (for H2) is located near $b/a = 2.5$ where $C = 2.389$; however, the Nusselt number values as given in [9], for the H2 case, behaves differently.

Table 1
Effective values of parameter C and $Nu_{D,FD}$ for rectangular ducts

b/a	C (for H1) Eq. (33)	C (for H2) Eq. (35)	$[h(2a)/k]_{FD}$ Eq. (19)	$Nu_{D,FD}$ Eq. (19)
1	3.325	2.906	3.608	3.608
1.2	3.069	2.684	3.342	3.646
1.5	2.866	2.511	3.159	3.790
2	2.731	2.406	3.092	4.123
3	2.689	2.404	3.197	4.795
4	2.711	2.457	3.332	5.331
5	2.739	2.512	3.443	5.738
6	2.766	2.560	3.529	6.049
7	2.788	2.600	3.597	6.294
8	2.807	2.635	3.651	6.490
9	2.823	2.664	3.695	6.651
10	2.837	2.689	3.732	6.785
15	2.883	2.775	3.849	7.217
20	2.909	2.824	3.912	7.451
∞	3.000	3.000	4.118	8.235

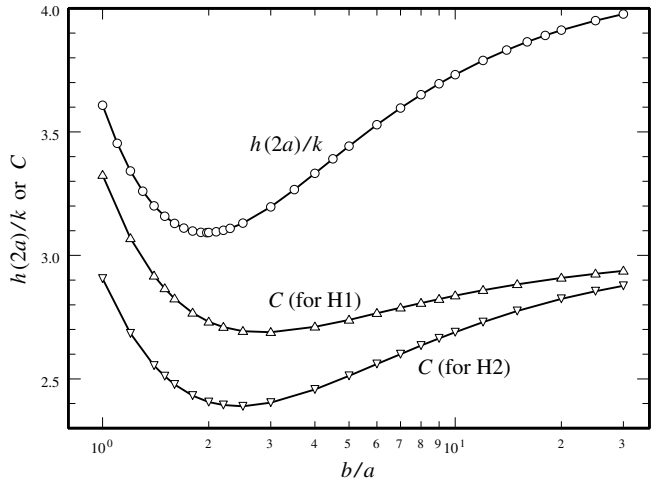

Fig. 2. The variation of thermally fully developed heat transfer coefficient for H1 case and the effective dimensionless velocity slope C for H1 case, Eq. (33), and H2 case, Eq. (55), versus b/a, for flow in rectangular ducts.

From this point forward, the emphasis of this work is devoted mainly to the H1 case. It was noted that the C parameter for H1 is the same as that for the locally constant wall temperature case in [10]. For that case, the inclusion of an additional term improved the accuracy of Eq. (36b) at relatively larger distance from the entrance location [10]; that is,

$$\frac{ha}{k}=\frac{0.651(C)^{1/3}}{(x)^{1/3}[1+e(x)^{1/3}]} \tag{37a}$$

and the estimated value of e, as given in [10], is

$$e=0.151+\frac{0.58}{\bar{b}} \tag{37b}$$

It should be stated that Eq. (37a) was successfully tested for the H2 case and the Nusselt number results agreed well with those in [11]. A mid-range comparison indicated the existence of a larger curvature effect [10] due to higher temperature values at the corners that may require increasing the parameter e in Eq. (37b).

3.3. Entrance formulation at large x

When the axial distance is not very small, a different methodology is needed to obtain a relatively accurate solution to this problem. The alternative Green's function solution in [12, Section 10.3] is selected for this study. Using a modified dimensionless temperature

$$\theta^*(y,z;x)=\theta(y,z;x)-\theta_w(x) \tag{38}$$

and after replacing $\theta(y,z;x)$ in the energy equation, Eq. (13), it becomes

$$\frac{\partial^2\theta^*}{\partial y^2}+\frac{\partial^2\theta^*}{\partial z^2}-\frac{\bar{u}}{\overline{U}}\frac{d\theta_w}{dx}=\frac{\bar{u}}{\overline{U}}\frac{\partial\theta^*}{\partial x} \tag{39}$$

with the inlet and the boundary conditions $\theta^*(y,z;0)=\theta^*(\pm1,z;x)=\theta^*(y,\pm\bar{b};x)=0$. The parameter $d\theta_w(x)/dx$ appearing in this equation serves as a heat sink. Then, the temperature solution [12, Eq. (10.77)] is

$$\begin{aligned}\theta^*(y,z;x)&=\theta(y,z;x)-\theta_w(x)\\&=-\int_{\xi=0}^{x}\int_{z'=0}^{\bar{b}}\int_{y'=0}^{1}\left(\frac{\bar{u}(y',z')}{\overline{U}}\right)\left(\frac{d\theta_w(\xi)}{d\xi}\right)\\&\quad\times G(y,z,x|y',z',\xi)\,dy'\,dz'\,d\xi\end{aligned} \tag{40}$$

Next, using the corresponding mean temperature

$$\theta_m^*(x)=\frac{1}{\bar{b}\times1}\int_{z=0}^{\bar{b}}\int_{y=0}^{1}\left(\frac{\bar{u}(y,z)}{\overline{U}}\right)\theta^*(y,z;x)\,dy\,dz \tag{41}$$

leads to the relation

$$\begin{aligned}&\theta_m(x)-\theta_w(x)\\&=-\frac{1}{\bar{b}}\int_{z=0}^{\bar{b}}\int_{y=0}^{1}\int_{\xi=0}^{x}\int_{z'=0}^{\bar{b}}\int_{y'=0}^{1}\left(\frac{\bar{u}(y',z')}{\overline{U}}\right)\\&\quad\times\left(\frac{d\theta_w(\xi)}{d\xi}\right)\left(\frac{\bar{u}(y,z)}{\overline{U}}\right)G(y,z,x|y',z',\xi)\,dy'\,dz'\,d\xi\,dy\,dz\end{aligned} \tag{42}$$

As shown in Eq. (42), the Green's function is integrated over y, y', z, and z' to get the function

$$\begin{aligned}\Gamma(x-\xi)&=\frac{1}{(\bar{b})^2}\int_{z=0}^{\bar{b}}\int_{y=0}^{1}\int_{z'=0}^{\bar{b}}\int_{y'=0}^{1}\left(\frac{\bar{u}(y',z')}{\overline{U}}\right)\left(\frac{\bar{u}(y,z)}{\overline{U}}\right)\\&\quad\times G(y,z,x|y',z',\xi)\,dy'\,dz'\,dy\,dz\end{aligned} \tag{43}$$

This selection simplifies the form of Eq. (42) and it becomes

$$\theta_m(x)-\theta_w(x)=-(\bar{b}\times1)\int_{\xi=0}^{x}\left(\frac{d\theta_w(\xi)}{d\xi}\right)\Gamma(x-\xi)\,d\xi \tag{44}$$

It is sometimes analytically possible to determine $\theta_w(x)$ from Eq. (26) by using the Laplace transform method, since the right side is the convolution integral. For special cases depending on the functional form of $\Gamma(x)$; e.g., for slug flow in passages, the solutions become the same as those for thermal conduction in solids as discussed in

[13]. Also, it is possible to get a numerical solution with an inverse procedure that uses the function specification method.

The Green's function used in this formulation, as given in [12,14, Eq. (10.55)], is

$$G(y,z,x|y',z',\xi)=\sum_{m=1}^{N}\Phi_m(y',z')\Psi_m(y,z)\mathrm{e}^{-\lambda_m^2(x-\xi)} \tag{45a}$$

wherein

$$\Psi_m(y,z)=\sum_{j=1}^{N}d_{mj}f_j(y,z) \tag{45b}$$

and

$$\Phi_m(y',z')=\sum_{j=1}^{N}p_{mi}f_j(y',z') \tag{45c}$$

The basis functions $f_j(y,z)$ in Eqs. (45b–c) are members of a complete set, each satisfying the boundary condition of the first kind; therefore, the relation

$$f_j=(1-\bar{y}^2)(\bar{b}^2-\bar{z}^2)\bar{y}^{2(m_j-1)}\bar{z}^{2(n_j-1)};\quad \text{for } j=1,2,\ldots,N \tag{46}$$

for all combinations of m_j and n_j represents a suitable set of basis functions. This would make the exponents m_j and n_j for $j=1,2,3,4,5,6,\ldots$ to become $(m_1,n_1)=(1,1)$, $(m_2,n_2)=(2,1)$, $(m_3,n_3)=(1,2)$, $(m_4,n_4)=(3,1)$, $(m_5,n_5)=(2,2)$, $(m_6,n_6)=(1,3),\ldots$ Therefore, for a complete set, N depends on the range of m_j and n_j. After selection of $f_j(y,z)$, the members of matrices **A** and **B** are

$$a_{ij}=-\int_{\bar{z}=0}^{\bar{b}}\int_{\bar{y}=0}^{1}\nabla f_{\mathrm{i}}(\bar{y},\bar{z})\cdot\nabla f_j(y,z)\mathrm{d}y\,\mathrm{d}z \tag{47a}$$

and

$$b_{ij}=\int_{\bar{z}=0}^{\bar{b}}\int_{\bar{y}=0}^{1}\left(\frac{\bar{u}}{\overline{\overline{U}}}\right)f_{\mathrm{i}}(y,z)f_j(y,z)\mathrm{d}y\,\mathrm{d}z \tag{47b}$$

Once the matrices **A** and **B** are known, the relation

$$(\mathbf{A}+\lambda_m^2\mathbf{B})\cdot\mathbf{d}_m=0 \tag{48}$$

provides the eigenvalues λ_m^2, and coefficients d_{jm}. The eigenvectors $\mathbf{d}_m$ contains d_{jm}, for all j values, and it will constitute the rows of a matrix **D** for insertion in equation

$$\mathbf{P}=[(\mathbf{D}\cdot\mathbf{B})^{\mathrm{T}}]^{-1} \tag{49}$$

that is the product of matrices **D** and **B** transposed and then inverted. The computed matrix **P** has the members p_{mj} for inclusion in Eq. (45c).

3.3.1. The function specification method

When x is relatively large, a solution is obtainable using a parameter estimation procedure that uses a reduced form of Eq. (43)

$$\Gamma(x-\xi)=\sum_{m=1}^{N}\left[\frac{1}{\bar{b}}\int_{z'=0}^{\bar{b}}\int_{y'=0}^{1}\left(\frac{\bar{u}(y',z')}{\overline{\overline{U}}}\right)\Phi_m(y',z')\mathrm{d}y'\,\mathrm{d}z'\right]\times\left[\frac{1}{\bar{b}}\int_{z'=0}^{\bar{b}}\int_{y'=0}^{1}\left(\frac{\bar{u}(y,z)}{\overline{\overline{U}}}\right)\Psi_m(y,z)\mathrm{d}y\,\mathrm{d}z\right]\mathrm{e}^{-\lambda_m^2(x-\xi)} \tag{50}$$

and, in a shorthand form, Eq. (50) is rewritten as

$$\Gamma(x-\xi)=\sum_{m=1}^{N}\overline{\Phi}_m\overline{\Psi}_m\mathrm{e}^{-\lambda_m^2(x-\xi)} \tag{51}$$

wherein these averaged quantities are

$$\overline{\Phi}_m=\frac{1}{\bar{b}}\int_{z'=0}^{\bar{b}}\int_{y'=0}^{1}\left(\frac{\bar{u}(y',z')}{\overline{\overline{U}}}\right)\Phi_m(y',z')\mathrm{d}y'\,\mathrm{d}z' \tag{52a}$$

and

$$\overline{\Psi}_m=\frac{1}{\bar{b}}\int_{z'=0}^{\bar{b}}\int_{y'=0}^{1}\left(\frac{\bar{u}(y,z)}{\overline{\overline{U}}}\right)\Psi_m(y,z)\mathrm{d}y\,\mathrm{d}z \tag{52b}$$

Eq. (44) after substitution of $\Gamma(x-\xi)$ reduces to

$$\theta_m(x)-\theta_{\mathrm{w}}(x)=-\bar{b}\sum_{m=1}^{N}\int_{\xi=0}^{x}\left(\frac{\mathrm{d}\theta_{\mathrm{w}}(x)}{\mathrm{d}x}\right)\overline{\Phi}_m\overline{\Psi}_m\exp[-\lambda_m^2(x-\xi)]\mathrm{d}\xi \tag{53}$$

for inverse estimation of $\theta_{\mathrm{w}}(x)$. The function specifications method in Beck et al. [15,16] is a suitable technique.

In accordance with the function specifications method [15,16], the physics of this problem suggests using the wall temperature θ_{w} to have the following form:

$$\theta_{\mathrm{w}}(x)=\delta+\frac{1+\bar{b}}{\bar{b}}x+\sum_{j=1}^{M}c_j\phi_j(x). \tag{54}$$

Following the appropriate substitution of $\theta_{\mathrm{w}}(x)$ in Eq. (54), the result is

$$\theta_m(x)-\left(\delta+\frac{1+\bar{b}}{\bar{b}}x+\sum_{j=1}^{M}c_j\phi_j(x)\right)=-\bar{b}\sum_{m=1}^{N}\overline{\Phi}_m\overline{\Psi}_m\int_{\xi=0}^{x}\exp[-\lambda_m^2(x-\xi)]\times\left(\frac{1+\bar{b}}{\bar{b}}+\sum_{j=1}^{M}c_j\frac{\mathrm{d}\phi_j(x)}{\mathrm{d}x}\right)\mathrm{d}\xi \tag{55}$$

The parameter δ in Eqs. (54) and (55) represents the quantity $\theta_{\mathrm{w}}(x)-\theta_m(x)$ as x becomes very large, while $\theta_m(x)=(1+\bar{b})x/\bar{b}$. As shown by Eq. (18), $\delta=-\theta_m^*$ and, therefore, it can be determined using the fully developed solution of the temperature field. Then, Eq. (54) suggests that all $\phi_j(x)$ functions should vanish as x becomes large and this condition makes $\phi_j(x)$ functions to be viewed as exponentially decaying functions. The next step is to compute the constants c_j using an appropriate inverse estimation methodology.

Since $\theta_m(x) = (1+\bar{b})x/\bar{b}$, the left side of Eq. (55) is

$$\theta_m(x) - \theta_w(x) = -\delta - \sum_{j=1}^{M} c_j \phi_j(x) \tag{56}$$

and then it reduces to

$$-\bar{b}\sum_{m=1}^{N} \overline{\Phi}_m \overline{\Psi}_m \int_{\xi=0}^{x} \left[\frac{1+\bar{b}}{\bar{b}} + \sum_{j=1}^{M} c_j \frac{\mathrm{d}\phi_j(\xi)}{\mathrm{d}\xi}\right] \times \exp[-\lambda_m^2(x-\xi)]\,\mathrm{d}\xi = -\delta - \sum_{j=1}^{M} c_j \phi_j(x) \tag{57}$$

By rearranging the terms, Eq. (57) assumes a suitable form for the evaluation of c_j coefficients, that is,

$$\sum_{j=1}^{M} c_j \left\{ \phi_j(x) - \bar{b}\sum_{m=1}^{N} \overline{\Phi}_m \overline{\Psi}_m \int_{\xi=0}^{x} \left[\frac{\mathrm{d}\phi_j(\xi)}{\mathrm{d}\xi}\right] \exp[-\lambda_m^2(x-\xi)]\,\mathrm{d}\xi \right\} = -\delta + \bar{b}\left(\frac{1+\bar{b}}{\bar{b}}\right) \sum_{m=1}^{N} \overline{\Phi}_m \overline{\Psi}_m \frac{1-\exp[-\lambda_m^2 x]}{\lambda_m^2} = -\bar{b}\left(\frac{1+\bar{b}}{\bar{b}}\right) \sum_{m=1}^{N} \overline{\Phi}_m \overline{\Psi}_m \frac{\exp[-\lambda_m^2 x]}{\lambda_m^2} \tag{58}$$

It is to be noted that the left side of Eq. (58) vanishes as $x \to \infty$ since $\phi_j(x)$ in Eq. (56) decays exponentially as $x \to \infty$. This implies that the right side must also become equal to zero as $x \to \infty$. Therefore, the sum of all constants (including δ) on the right side of Eq. (58) is equal to zero and they are discarded.

As stated earlier, the inverse procedure begins by selecting a set of suitable $\phi_j(x)$ functions. As suggested by Eq. (56), the quantity within the summation has a finite value of $-\delta$ at $x = 0$ and goes zero as x becomes infinite. The arbitrarily selected $\phi_j(x)$ functions have the form $\phi_j(x) = \exp(-j^2\pi^2 x)$ that performed well at large values of x. The small-x solution, Eq. (36a), shows that $\mathrm{d}\theta_w(x)/\mathrm{d}x \to \infty$ as $x \to 0$. Accordingly, this set of functions is augmented by another function that behaves as dictated by Eq. (36a) when x goes toward zero and vanishes as x goes to infinity. The selected functions are

$$\phi_1 = \mathrm{e}^{-\pi\sqrt[3]{x}} \tag{59a}$$

$$\phi_j = \mathrm{e}^{-(j-1)^2(\pi^2 x)} \quad \text{for } j = 2, 3, \ldots \tag{59b}$$

wherein the function ϕ_1 has a proper slope of $+\infty$ when $x \to 0$ if the corresponding computed coefficient c_1 in Eq. (56) has a negative value.

The next task is the determination of the coefficients, c_j, for $j = 1, 2, \ldots, M$, on the left side of Eq. (58). The procedure is to evaluate the terms in Eq. (58) at N_p different values of $x = x_i$ within a specified range. The coefficients on the left side of Eq. (58) will constitute the elements of a new matrix $\mathbf{A}$ and they are

$$a_{ij} = \phi_j(x_i) - \bar{b}\int_{\xi=0}^{x_i} \left[\frac{\mathrm{d}\phi_j(\xi)}{\mathrm{d}\xi}\right] \sum_{m=1}^{N} \overline{\Phi}_m \overline{\Psi}_m \exp[-\lambda_m^2(x_i-\xi)]\,\mathrm{d}\xi \tag{60}$$

for $i = 1, 2, \ldots, N_p$, and $j = 1, \ldots, M$. Also, the computed parameter on the right side of Eq. (58)

$$\omega_i = -\bar{b}\left(\frac{1+\bar{b}}{\bar{b}}\right) \sum_{m=1}^{N} \overline{\Phi}_m \overline{\Psi}_m \frac{\exp[-\lambda_m^2(x_i)]}{\lambda_m^2} \tag{61}$$

are the members of vector $\mathbf{\Omega}$. Finally, the results are summarized in the matrix form as

$$[\mathbf{A}]\{\mathbf{C}\} = \{\Omega\} \tag{62}$$

This equation stands for Eq. (58) for the determination of coefficients $c_1, c_2, c_3, \ldots, c_M$, the members of vector $\mathbf{C}$. When the number of points $N_p > M$, a standard least squares procedure yields the solution

$$\{\mathbf{C}\} = [\mathbf{A}^{\mathrm{T}}\mathbf{A}]^{-1}\{\mathbf{A}^{\mathrm{T}}\Omega\} \tag{63}$$

Once the vector $\mathbf{C}$ is known, the wall temperature is available from Eq. (54) and the local temperature from Eq. (40).

4. Results and discussion

Before using this formulation to calculate temperature values, it is necessary to show that this Green's function solution can provide sufficiently accurate results. To test its accuracy, the fully developed solution was used to determine θ_m^* from the exact series solution in Eq. (18) and then the Nusselt number from Eq. (19). Alternatively, the corresponding solution of θ_m^* by the extended weighted residual is

$$(\theta_m^*)_{\mathrm{FD}} = -(1+\bar{b})\sum_{m=1}^{N} \frac{\overline{\Phi}_m \overline{\Psi}_m}{\lambda_m^2} \tag{64}$$

that would yield the Nusselt number using Eq. (19). Table 2 compares the computed Nusselt numbers obtained by these two methods. The data in column 2 are from Eqs. (18) and (19) and those in columns 3, 4, and 5 are for $N = 21, 36$, and 55 terms using Eqs. (64) and (19). For sufficient accuracy, $N = 55$ is used when $b/a = 10$, and for the remaining aspect ratios $N = 36$ is the selection, in the subsequent analysis.

The evaluation of the accuracy of this inverse procedure is an interesting issue. Following the computation of θ_w by this inverse procedure, it is inserted in Eq. (42) to determine the mean or bulk temperature. Since the exact value of mean temperature $\theta_m = (1+\bar{b})x/\bar{b}$ is readily known, the percent error

Table 2
A comparison of the exact Nusselt number $Nu_{D,FD} = hD_h/k$ computed by utilizing Eq. (18), and the one from Eq. (64)

b/a	Exact	$N = 21$	$N = 36$	$N = 55$
1	3.60795	3.60793	3.60795	3.60795
2	4.12330	4.12327	4.12330	4.12330
3	4.79479	4.79474	4.79479	4.79479
4	5.33107	5.33097	5.33105	5.33107
5	5.73769	5.73753	5.73767	5.73769
7	6.29405	6.29371	6.29401	6.29404
10	6.78497	6.78437	6.78486	6.78495

$$\varepsilon = \frac{(\theta_m)_{\text{Calc.}} - (1+\bar{b})x/\bar{b}}{(1+\bar{b})x/\bar{b}} \times 100 \tag{65}$$

is an indicative of the numerical accuracy. This is an instance of intrinsic verification [17]. Fig. 3 shows the computed percent error in θ_m for four sets of results in four regions along x-axis. Each set of values was computed using ~500 unequally-spaced locations within a range of the dimensionless axial coordinate. Two essential sets are selected so that $0.0001 \leqslant x \leqslant 0.06$ for the first set and $0.0001 \leqslant x \leqslant 0.3$ for the second set. The higher values of x were emphasized in two additional sets. Fig. 3 shows a summary of the results for different b/a values. As can be seen from Fig. 3a and b, the error in less than 0.1%, except when $x < 0.005$. Fig. 4a is a representative sample of data that illustrates the reason for having multiregions. For $b/a = 2$, Fig. 4a shows small error at lower values of x for the first solution when $0.0001 \leqslant x \leqslant 0.06$. The second solution also begins at $x = 0.0001$ but the range of x is extended to $x = 0.3$. The data plotted in this figure show that the error increases at the lower values of x but eventually reduces to below 0.1% for $x > 0.06$, where it is needed. Fig. 4b is prepared to demonstrate the effect of this larger error on the computed θ_w. Although, Fig. 4a shows that the errors in second solution, at small x values, are much larger, the data in Fig. 4b show only small differences in

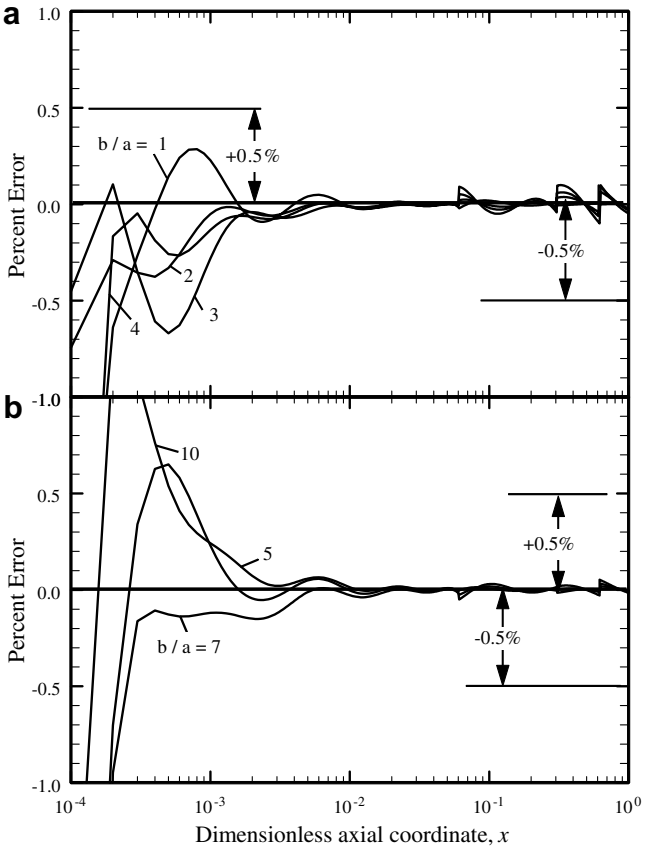

Fig. 3. Estimated percent error ε, Eq. (65), for $b/a = 1$, 2, 3, 4, 5, 7, and 10.

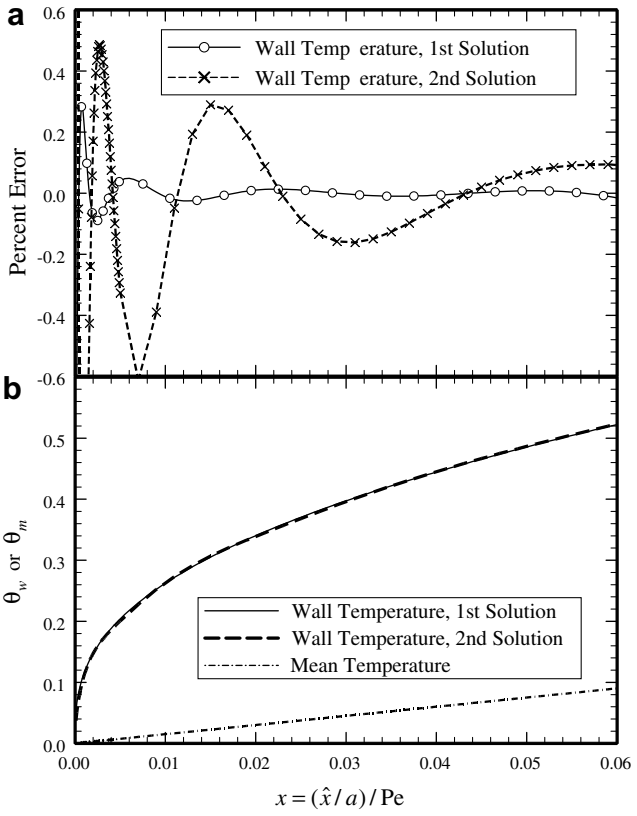

Fig. 4. A sample comparison of the first and the second solutions for $b/a = 2$ emphasizing different ranges of the axial coordinate x: (a) the percent error ε, Eq. (65), and (b) the wall temperature θ_w, Eq. (54).

the θ_w values. A sample of the computed large-x Nusselt number, Nu_D, data is presented in Table 3. At larger values of x, the error is mainly the truncation error. Also, at smaller values of x, above 10^{-3}, the error remains relatively small and gradually increases as x decreases.

It is appropriate to view a comparison between the small-x and large-x solutions. Fig. 5a shows that the solid lines (large x) perform properly when $x \geqslant 0.001$ as they approach the dash lines (small x). Also, the dash lines properly assume similar values in the neighborhood of $x = 0.001$, an indicative of their accuracy as $x \to 0$. For comparison, the Nusselt number values from Kays and Crawford [3] are also plotted in Fig. 5a. There are detectable differences between these computed data and those from [3]. Table 4 shows the relative values of the results from this study and those from [3, Tables 9 and 10]. In this table, the dimensionless axial coordinate is selected to be $x^+ = 2(\hat{x}/D_h)/(PrRe_D)$ as used in [3]; therefore, $x^+ = x(D_h/a)^2/2$ for the data in Table 2. Except at few isolated locations the differences in the tabulated values are relatively small.

The small-x solution, Eq. (36b), and data plotted in Fig. 2 hint toward the feasibility of having a unique correlation that would provide an acceptable simple relation for the Nusselt number within the broad range of $0 < x < \infty$ and $1 \leqslant b/a < \infty$. Accordingly, a correlation is prepared that can accomplish this task, it is

Table 3
A sample of Nusselt number, Nu_D, at larger values of x, computed using Eq. (56) in the function specification method

x	$b/a=1$	$b/a=2$	$b/a=3$	$b/a=4$	$b/a=5$	$b/a=7$	$b/a=10$	$b/a=\infty$
0.0007	20.82	26.53	29.70	31.41	32.75	34.89	36.71	42.25
0.001	18.51	23.47	26.44	28.10	29.29	31.10	32.76	37.55
0.002	14.64	18.49	20.98	22.51	23.49	24.82	26.17	29.89
0.003	12.74	16.11	18.26	19.68	20.60	21.74	22.92	26.18
0.004	11.54	14.62	16.55	17.88	18.75	19.81	20.87	23.85
0.005	10.71	13.57	15.35	16.59	17.44	18.45	19.43	22.20
0.007	10.07	12.13	13.73	14.83	15.63	16.59	17.47	19.94
0.01	8.512	10.78	12.23	13.20	13.92	14.83	15.62	17.82
0.02	6.798	8.594	9.789	10.59	11.15	11.93	12.57	14.43
0.03	6.005	7.569	8.634	9.36	9.871	10.56	11.15	12.84
0.04	5.514	6.934	7.920	8.598	9.077	9.715	10.27	11.86
0.05	5.177	6.494	7.425	8.068	8.527	9.130	9.657	11.18
0.07	4.737	5.912	6.772	7.371	7.802	8.369	8.865	10.30
0.1	4.352	5.399	6.196	6.755	7.160	7.697	8.165	9.530
0.2	3.844	4.652	5.376	5.901	6.285	6.803	7.255	8.574
0.3	3.690	4.406	5.106	5.623	6.005	6.522	6.975	8.332
0.4	3.638	4.272	4.969	5.494	5.884	6.414	6.880	8.263
0.5	3.619	4.223	4.914	5.441	5.834	6.368	6.839	8.244
0.7	3.609	4.162	4.848	5.381	5.781	6.327	6.808	8.236
1.0	3.608	4.145	4.825	5.359	5.762	6.312	6.797	8.235
1.2	3.608	4.139	4.817	5.352	5.756	6.307	6.794	8.235
∞	3.608	4.123	4.795	5.331	5.738	6.294	6.785	8.235

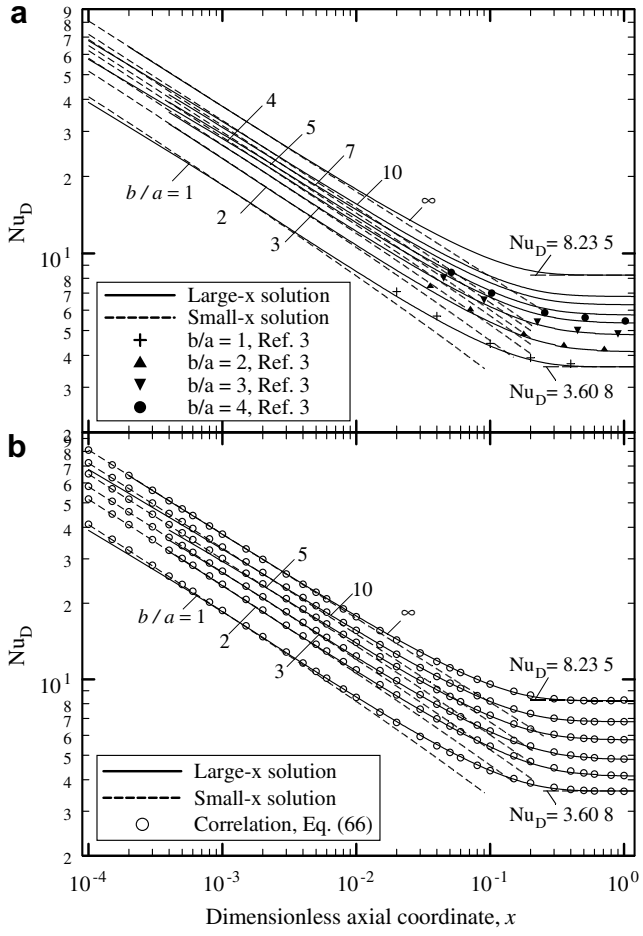

Fig. 5. Computed small-x and large-x Nusselt numbers versus $x=(\hat{x}/a)/Pe$ and their comparison with (a) data from [3] and (b) new correlation, Eq. (66).

Table 4
A numerical comparison between present calculations and those from [3], within the parentheses

x^+	$b/a=1$	$b/a=2$	$b/a=3$	$b/a=4$	$b/a=\infty$
0	∞	∞	∞	∞	∞
0.01	6.824	7.057	7.667	8.045	9.9878
	(7.10)	(7.46)	(8.02)	(8.44)	
0.02	5.544	5.929	6.356	6.719	8.8031
	(5.69)	(6.05)	(6.57)	(7.00)	(8.80)
0.05	4.352	4.762	5.285	5.670	8.2634
	(4.45)	(4.84)	(5.39)	(5.87)	
0.10	3.845	4.299	4.943	5.421	8.2355
	(3.91)	(4.38)	(5.00)	(5.62)	(8.25)
0.20	3.638	4.173	4.839	5.360	8.2355
	(3.71)	(4.22)	(4.85)	(5.45)	
∞	3.608	4.123	4.795	5.331	8.2353
	(3.60)	(4.11)	(4.77)	(5.35)	(8.235)

$$Nu_D=\frac{hD_h}{k}=\frac{0.651(D_h/a)}{(x/C)^{1/3}+(0.58/\bar{b})(x/C)^{2/3}}+\frac{Nu_{D,FD}}{\left[1+\left(2.48-\frac{0.24}{\bar{b}^2}\right)(C^2x)^{-2/3}\right]^{4/3}}\quad \text{for } 0\leqslant x\leqslant 0.8$$
$$=Nu_{D,FD}\quad \text{for } 0.8<x<\infty \tag{66}$$

The second column of Table 1 contains the parameter C and $Nu_{D,FD}$ for insertion in Eq. (66). As an example, $C=3$ and $Nu_{D,FD}=8.235$ for parallel plate channels and the percent deviation using Eq. (66) is less than 1%. The symbols in Fig. 5b are representative values of the Nusselt numbers, acquired using Eq. (66). The circular symbols from this new correlation show excellent agreements with

the small-x solutions and good agreements with the large-x solutions.

5. Conclusion

The currently available heat transfer information related to the H1 boundary condition for rectangular ducts are for a relatively narrow range. Solutions provided herein for small-x and large-x values should enhance the available information in the heat transfer literature. These asymptotic solutions at very small x values have a broad range of applications and they can be used for ducts having other cross-section profiles. Similarly, the inverse methodology described herein also applies to ducts having other cross-section profiles. For completeness, a new correlation is provided that yields the Nusselt number for rectangular ducts with H1 boundary conditions, when $0 < x < \infty$ and $1 \leqslant b/a < \infty$.

References

[1] R.K. Shah, A.L. London, Laminar Flow Forced Convection in Ducts, Advances in Heat Transfer, Supplement 1, Academic Press, New York, 1978.
[2] W.M. Kays, M.E. Perkin, Forced convection internal flow in ducts, Section 7, in: W.M. Rohsenow, J.P. Hartnett (Eds.), Handbook of Heat Transfer, McGraw-Hill, New York, 1973.
[3] W.M. Kays, M.E. Crawford, Convective Heat and Mass Transfer, McGraw-Hill, New York, 1993.
[4] L.C. Burmeister, Convective Heat Transfer, second ed., John Wiley & Sons, New York, 1993.
[5] A. Bejan, Convection Heat Transfer, second ed., John Wiley & Sons, New York, 1982.
[6] R.V. Churchill, Fourier Series and Boundary Value Problems, McGraw-Hill, New York, 1941.
[7] M. Abramowitz, I.A. Stegun, Handbook of Mathematical Functions, National Bureau of Standards Applied Mathematics Series (1965) 55.
[8] S. Wolfram, The Mathematica Book, forth ed., Cambridge University Press, Cambridge, UK, 1999.
[9] A. Haji-Sheikh, Fully developed heat transfer to fluid flow in rectangular passages filled with porous materials, J. Heat Transfer 128 (2006) 550–556.
[10] A. Haji-Sheikh, J.V. Beck, Entrance effect on heat transfer to laminar flow through passages, Int. J. Heat Mass Transfer 50 (2007) 3340–3350.
[11] A. Haji-Sheikh, D.A. Nield, K. Hooman, Heat transfer in the thermal entrance region for flow through rectangular porous passages, Int. J. Heat Mass Transfer 49 (2006) 3004–3015.
[12] J.V. Beck, K. Cole, A. Haji-Sheikh, B. Litkouhi, Heat Conduction Using Green's Functions, Hemisphere Publishing Corporation, Washington, DC, 1992.
[13] A. Haji-Sheikh, J.V. Beck, Inverse determination of wall temperature during constant energy input, J. Numer. Heat Transfer, Part A 50 (2006) 401–418.
[14] A. Haji-Sheikh, E.M. Sparrow, W.J. Minkowycz, Heat transfer to flow through porous passages using extended weighted residuals method – a Green's function solution, Int. J. Heat Mass Transfer 48 (2005) 1330–1349.
[15] J.V. Beck, B. Blackwell, C.R. St.Clair Jr., Inverse Heat Conduction: Ill-posed Problems, Wiley-Interscience, New York, 1985.
[16] J.V. Beck, B. Blackwell, A. Haji-Sheikh, Comparison of some inverse heat conduction methods using experimental data, Int. J. Heat Mass Transfer 39 (1996) 3649–3657.
[17] J.V. Beck, R. McMaster, K.J. Dowding, D.E. Amos, Intrinsic verification methods in linear heat conduction, Int. J. Heat Mass Transfer 49 (2006) 2984–2994.